Solidification microstructure of super-α_2 alloy prepared by gas atomization

R. XU*, Y. Y. CUI, D. LI
Institute of Metal Research, Academia Sinica, Shenyang 110015, People's Republic of China

D. M. XU, Q. C. LI, Z. Q. HU
Harbin Institute of Technology, Harbin 150001, People's Republic of China

Ti–25Al–10Nb–3V–1Mo alloy has been prepared by gas atomization with atomizing pressure above 8 MPa. The cooling rate of $5 \times 10^3 \sim 3 \times 10^5$ K s^{-1} was obtained according to secondary dendritic arm spacing, as the particle size is 30 $\sim$300 μm. It is known that in the big particles two dendrite morphologies can be found, cellular dendrite and well-developed dendrite, and in small particles there exists only well-developed dendrite. The surface of particles is characteristic of solidification that is identical to the observation on the cross-sectional views. The micrographs of cross-sectional views show that the big particles, whether of cellular dendrite or well-developed dendrite, solidify by multiple nucleation events while the small particles of well-developed dendrite solidify from a single nucleation event. The microstructure of the alloy consists of single β_0 phase.

1. Introduction

The solidification of gas-atomized alloy is considerably complicated and very difficult to investigate. First, the heat flow from the droplet to environment is three-dimensional so the heat transfer prior to and during solidification of the alloy is more complex than that in other rapid solidification techniques [1]. Then, the various sizes of particles that can be obtained in a gas atomization process, and the mass fraction of particles keep log–normal relationship with the particle size [2] which influences the cooling rate, nucleation temperature, the number of nuclei, and the mode of crystal growth.

Levi and co-workers [3, 4] had set up Newtonian and non-Newtonian (enthalpy) models for heat flow in atomized metal droplets; the latter addresses a non-uniform temperature distribution inside the droplets. Relationships were developed between the process parameters in atomization, the kinetics and the thermal history of the powder. They had described the solidification of atomized metal droplets such as Al, Ni and Fe using the models. The solidification of alloys is different from that of metals, mainly because of solute redistribution, though the melts are similar in the heat flow from the droplet to environment as cooling. In this paper, an attempt is made to give some understanding of the solidification of the atomized powders by analysing the crystalline morphology of super-α_2 alloy.

2. Experimental procedure

The nominal composition of the alloy was Ti–25Al–10Nb–3V–1Mo (at %). The raw materials for gas atomization was prepared by consumable vaccum melting. The alloy powder was produced by a gas-atomization equipment where the alloy was melted by arc in a water-cooled copper crucible, then atomized in the atmosphere of pure argon (Ar $>$ 99.999%) with pressure above 8 MPa. Before smelting, the melting and the atomizing chambers of the equipment had been evacuated below 6.67×10^{-3} Pa, then charged in pure argon to 0.05 MPa.

The particle surface morphology was observed in an S-360-type scanning electron microscope (SEM). The cross-sectional views of the particles etched in a solution of $HF:HNO_3:H_2O = 1:1:30$ were observed by using a Neophot-2 optical microscope. Thin foil samples were prepared by argon ion beam milling. The microstructure was examined by transmission electron microscopy (TEM) using a Philips EM420 analytical electron microscope operating at 100 kV.

3. Results

3.1. Surface morphology of the powder

Under SEM, the gas-atomized powders are all spherical, whether the particles are big or small (Fig. 1a). This is different from gas-atomized aluminium alloy

* Also at Harbin Institute of Technology, Harbin 150001, People's Republic of China.

0022–2461

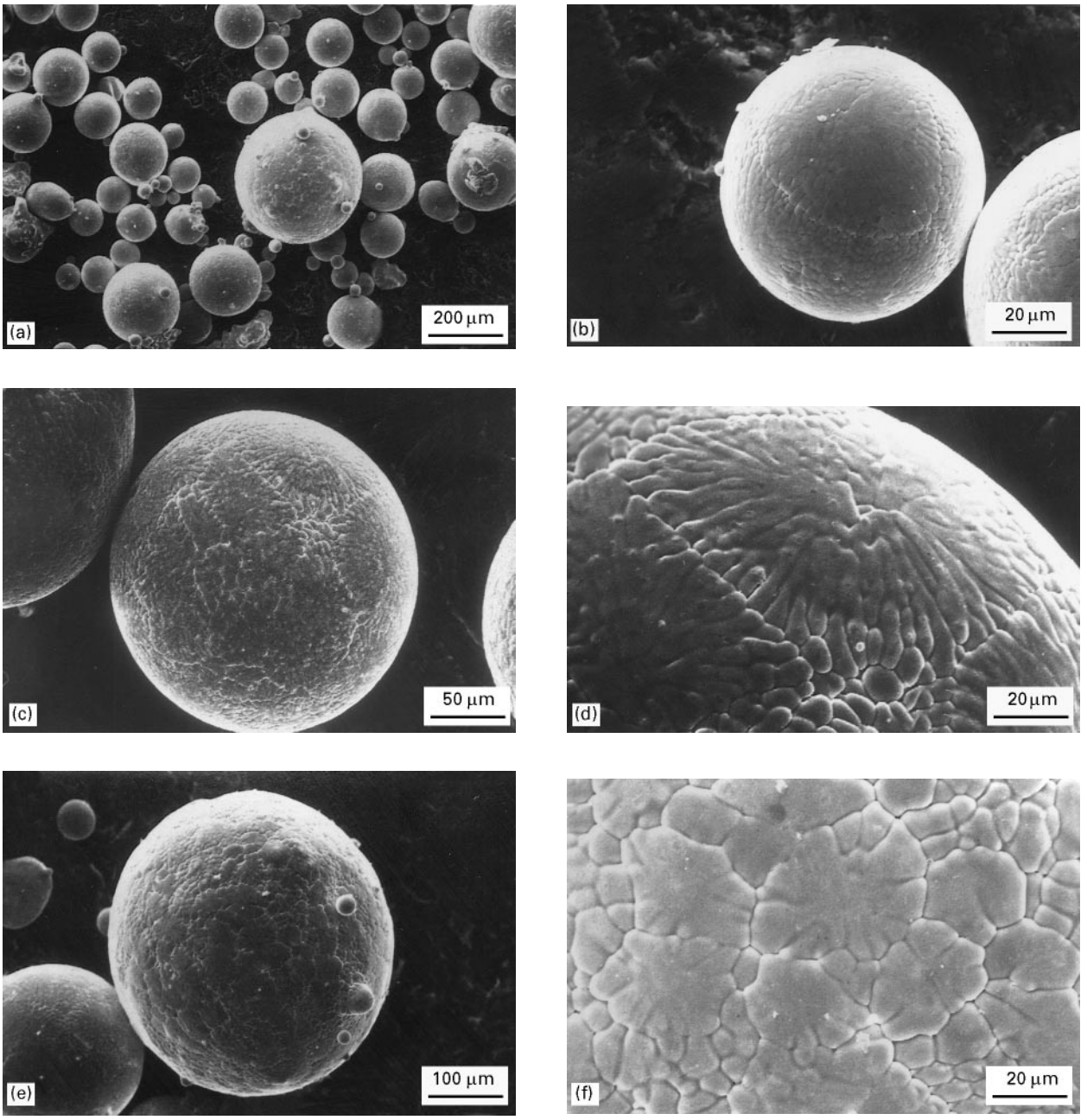

Figure 1 SEM micrographs of surface views. (a) Whole particles; (b) $d = 62$ μm; (c) and (d) $d = 143$ μm; (e) and (f) $d = 185$ μm. (b), (c) and (d) show well-developed dendrite and (e) and (f) cellular dendrite.

powder, of which the bigger particles are irregular [5]. The interacting force between the atoms of Ti_3Al-based alloy is strong and the surface tension of the alloy is high. So a droplet, which will solidify to form a particle, tends to be spherical during rapid solidification.

The particle surface of gas-atomized powder is a clear characteristic of solidification (Fig. 1). The β-grains with complete dendritic boundary were observed on the particle surface, where the secondary dendrite develops from the β-grain centre to the boundary. There are two different morphologies of β-dendrite in the particles. One is well-developed dendrite, as shown in Fig. 1b, c and d, with a flourishing secondary dendrite of uniform arm spacing and big β-grain of near rectangular boundary which is characteristic of body-centred cubic structure cystallization [6]. The other is similar to cellular dendrite with short secondary dendrites and small β-grains, as shown in Fig. 1e and f.

3.2. Cooling rate of the powder

The cooling rate of the particles depends strongly on the particle size. As shown in previous experiments, the cooling rate, in turn, has a relationship with the secondary dendritic arm spacing, and this relationship is independent of the preparation method. The results on plasma rotating electrode process (PREP) powder of Ti–25Al–10Nb–3V–1Mo alloy [7] had shown that the secondary dendritic arm spacing (S) has the relationship with the cooling rate as follows

$$S = 95.5\dot{T}^{-0.355}$$

where $\dot{T}$ is the cooling rate of the particles. The diameter of particles (d) and the secondary dendritic arm spacing were examined by SEM. The examined method of the arm spacing is the same as reference [7]. Fig. 2 shows the influence of particle size on the cooling rate of particles of Ti–25Al–10Nb–3V–1Mo alloy. The cooling rate above 5×10^3 K s^{-1} for the alloy is produced by the atomization process.

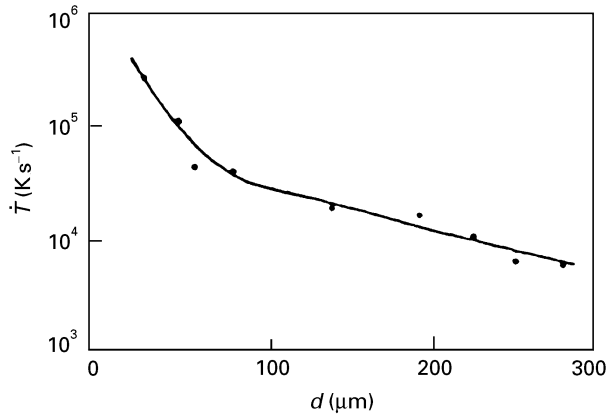

Figure 2 The cooling rate $\dot{T}$ versus size of particles, d.

3.3. Crystalline morphology of the alloy

The particle micrographs of cross-sectional views show not only the final structure morphology of alloy solidification but also the nucleation and growth of crystal during the solidifying process. Fig. 3 shows the micrographs of cross-sectional views of gas-atomized Ti_3Al-based alloy powder. The big particles can be divided into two kinds, according to their dendritic morphologies. One is the particles of well-developed dendrite, as shown Fig. 3c. Another is of cellular dendrite (Fig. 3d). The smaller the size of particles, the more the particles of the latter β-dendrite. When the size of particles is smaller than a certain value ($d \approx 70$ μm, $\dot{T} \approx 4 \times 10^4$ K s^{-1}), all particles have the solidified morphology of well-developed dendrite (Fig. 3b). For the particles of well-developed dendrite, the micrographs of cross-sectional views are somewhat different from the surface views in secondary dendrite morphologies. The secondary dendrites arrange non-regularly, and the above secondary dendrite can be found in the micrographs of cross-sectional views.

The nucleation position in the particles with cellular dendrite, which solidify by multiple nucleation events, cannot be found from the micrographs of

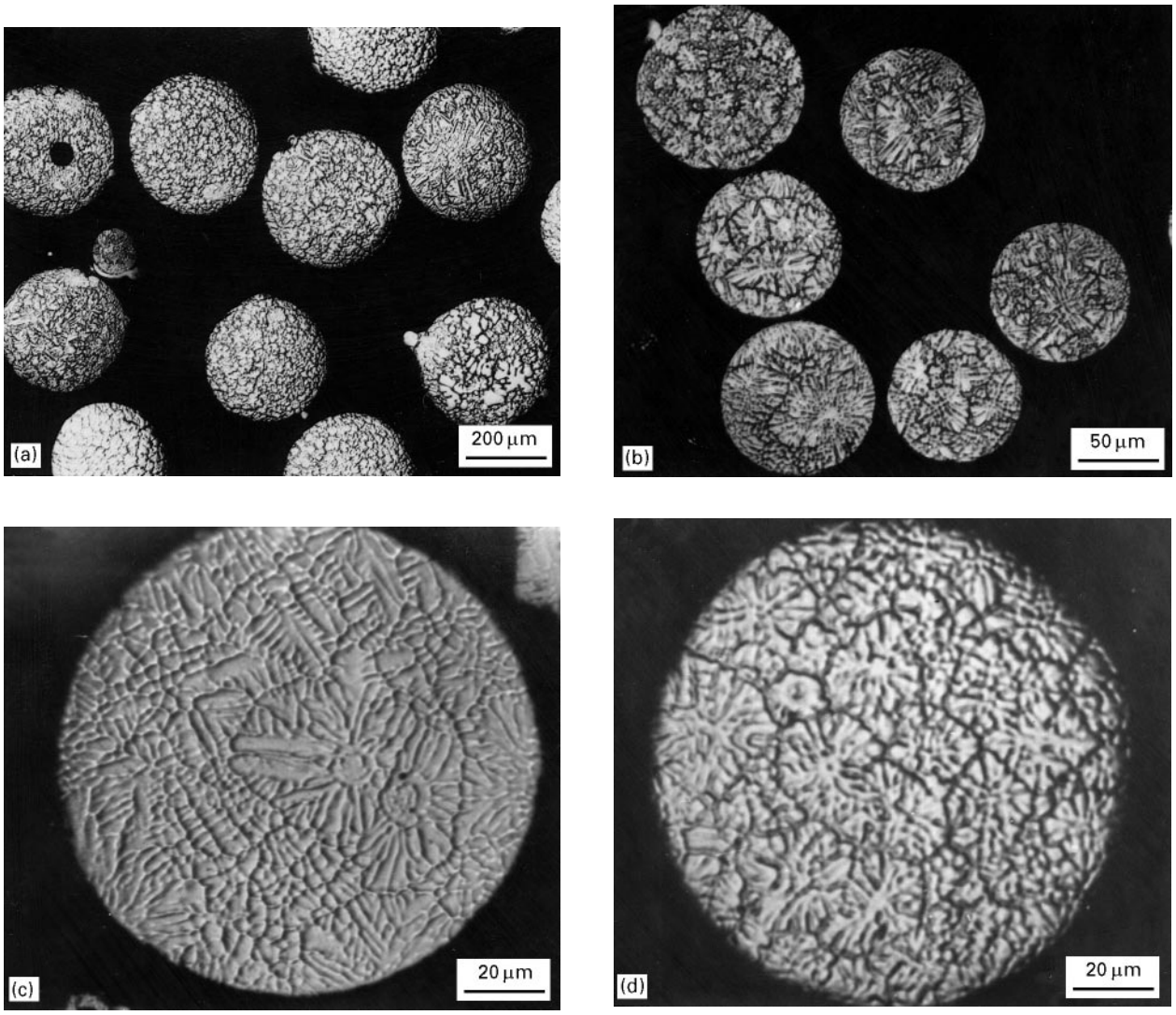

Figure 3 Optical micrographs of cross-sectional views. (a) 60 mesh ($d = 200 \approx 280$ μm); (b) 200 mesh ($d = 56 \approx 70$ μm); (c) showing well-developed dendrite; (d) showing cellular dendrite.

cross-sectional views. However, the position of nucleation and the direction of growth can be noticed in the particles with well-developed dendrite in the micrographs of cross-sectional views, as indicated with arrow. Of big particles well-developed dendrite, solidify by multiple nucleation events where crystal nucleates near the surface of droplets and develop to the centre, as shown in Fig. 4a and b. This can be also found in the fractograph of the particle, as in Fig. 5. Small particles solidify from a single nucleation event in which nucleation is also near the surface of droplets and develops radially, then a droplet solidifies into a particle, as shown in Fig. 4c and d.

3.4. Internal microstructure of the alloy

The internal microstructure of the alloy is examined using transmission electron microscopy and the selected area electron diffraction, as shown in Fig. 6. A network of thermal antiphase boundaries can be observed as a characteristic of ordered structure (Fig. 4a). Selected area electron patterns (Fig. 6c and d)

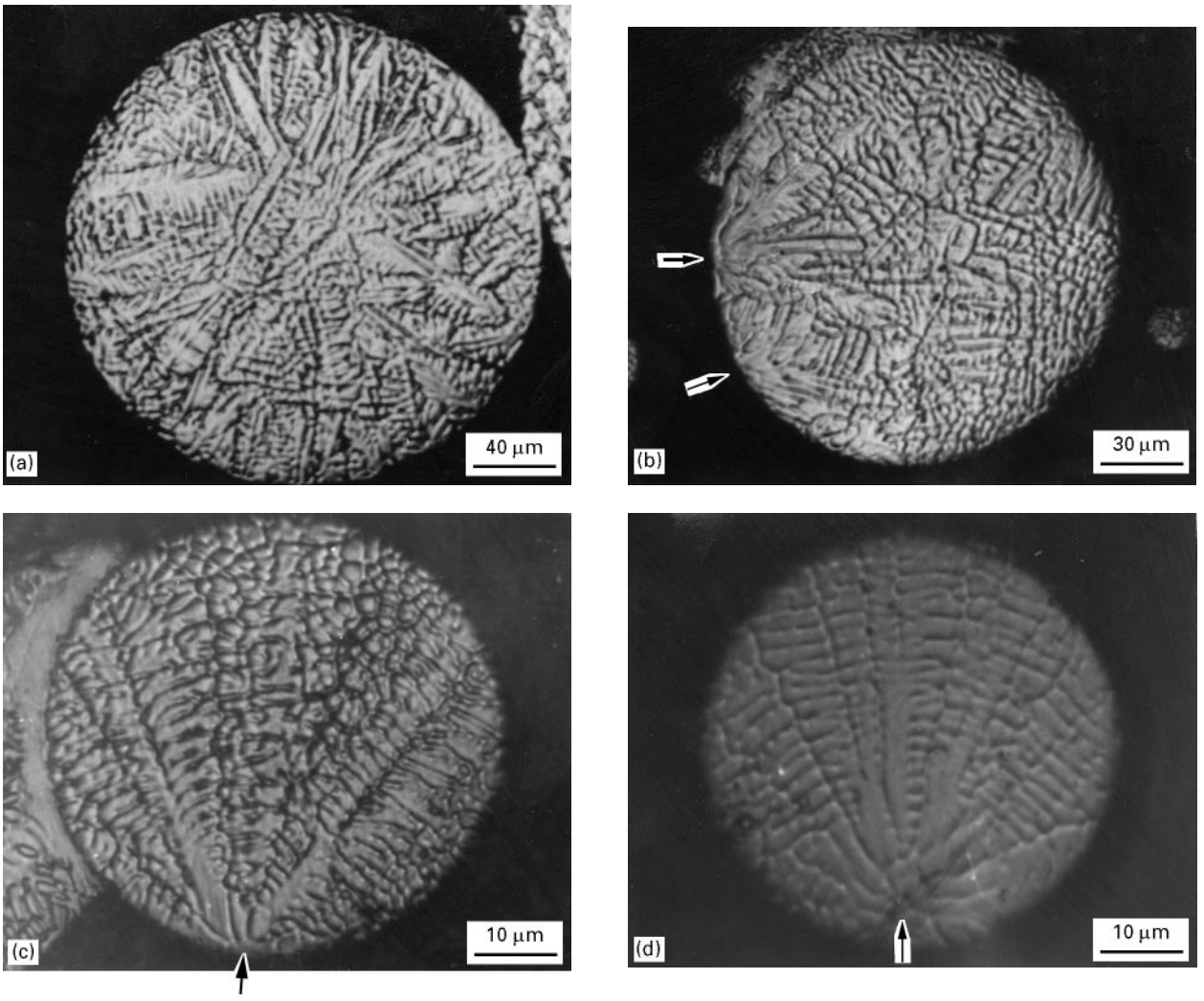

Figure 4 Optical micrographs of cross-sectional views showing nucleation and growth. (a) and (b) show multiple nucleation events; (c) and (d) show a single nucleation event. Arrows indicate the nucleation sites.

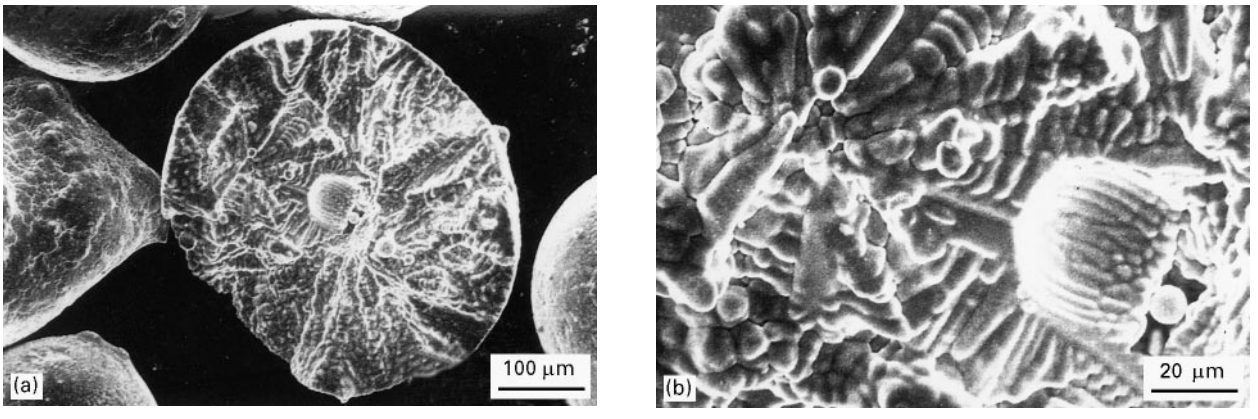

Figure 5 SEM fractographs of the particle showing nucleation and growth.

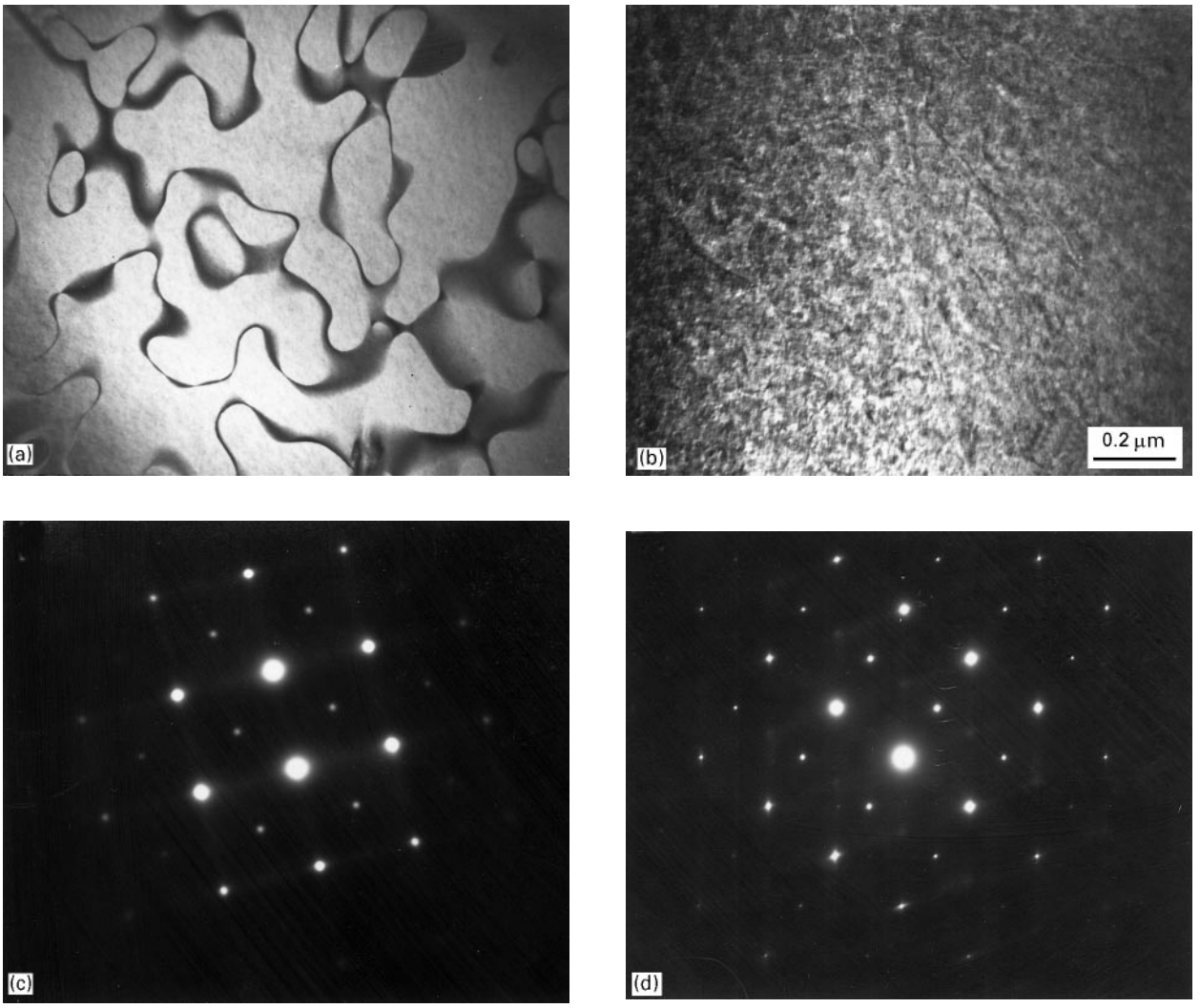

Figure 6 (a) TEM micrography showing antiphase boundaries in as-atomized alloy. (b) Bright-field two-beam image. (c) and (d) Selected area diffraction patterns [0 0 1] β and [0 1 1]β zone normal.

correspond to the β_0 phase which is the ordered derivative of β-phase, which refers to high-temperature disordered b.c.c phase. The examination of β zones such as $\langle 1\,0\,0 \rangle$ and $\langle 1\,1\,0 \rangle$ shows superlattice reflections characteristic of a B_2(CsCl) matrix. It is important for the observation of solidification morphology of the alloy, which would be impossible if the transformation of $\beta/\beta_0 \rightarrow \alpha/\alpha_2$ took place. Finer thermal antiphase boundaries and smaller grains can be obtained than in as-quenched one [8].

Strong streaking was observed along $\langle 1\,1\,0 \rangle$ and $\langle 1\,1\,2 \rangle$ β type direction and weak maxima at $\frac{1}{2}(1\,1\,0)$ and $\frac{1}{2}(1\,1\,2)$ β positions. When two-beam electron images were produced, contrast effects, as shown in Fig. 6b, were observed in the matrix. This type of matrix strain contrast corresponds to a "tweed" microstructure reported by Strychor *et al.* [9].

4. Discussion

4.1. Solute redistribution in the undercooled droplets

The crystalline morphology of an alloy is controlled by the distribution of solute and temperature inside the melt during solidification. In the models [10, 11] of solute trapping during rapid solidification, the parameter β is introduced into the expression of partition ratio for non-equilibrium solidification k_n, i.e. $\beta = Ra/D_i$, where R is the growth rate of crystal, a is average atomic distance, and D_i is the coefficient of atom diffusing along the solid/liquid interface, which is substituted approximately for the atom diffusion coefficient D_1 in melt. When $\beta \rightarrow 0$, $k_n \rightarrow k$ (k is equilibrium partition ratio); when $\beta > 0$, $k_n > k$ and k_n increased with k; $\beta \rightarrow \infty$, $k_n \rightarrow 1$ when solute is trapped and no structural feature appears in the alloy.

For Ti–25Al–10Nb–3V–1Mo alloy, when the cooling rate of rapid solidification is about $10^3 \sim 10^5$ K s^{-1}, R is the order of cm s^{-1} [7]. If D_1 is of the order of 10^{-5} cm^2 s^{-1} and a is taken as the lattice parameter of the alloy in the order of 10^{-8} cm, β is about the order of 10^{-3} which is near 0. This suggests that the solute redistributing exists during the solidification of gas atomized powder and the dendritic structure tends to form at the high solidification speed in the atomized droplets.

4.2. Temperature distribution and nucleation in the droplets

Levi and co-workers [3, 4] had set up two models of atomized droplets cooling – a Newtonian and

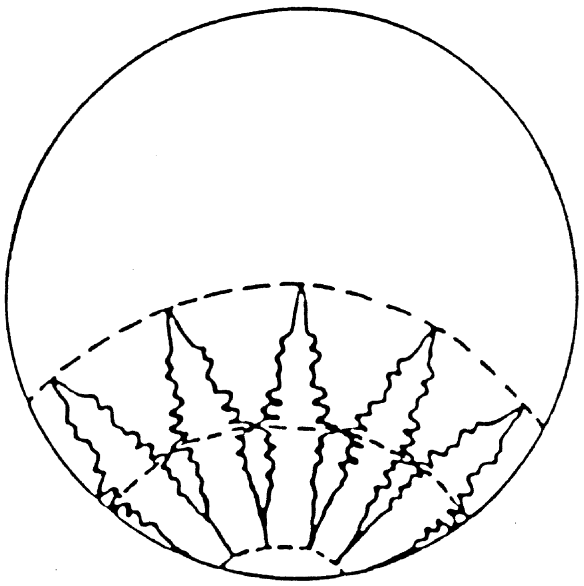

Figure 7 Schematic illustration of isotherm inside the particle (droplets).

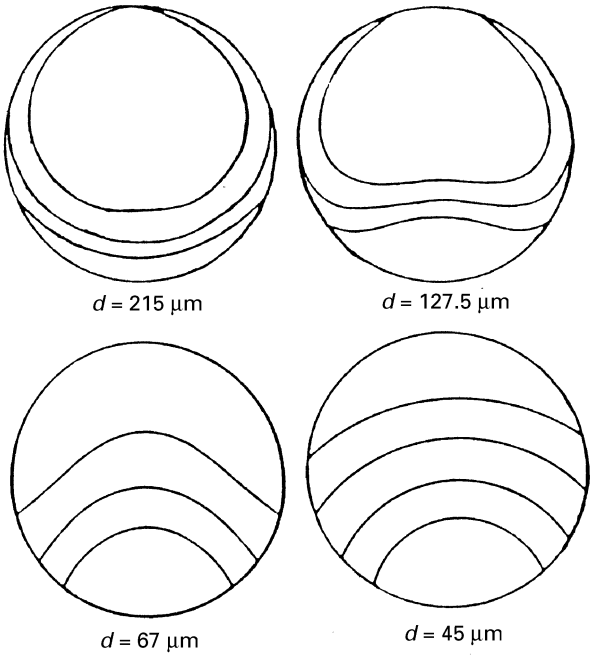

Figure 8 Isotherm inside the particles (droplets) obtained according to the dendrite, as shown in Fig. 4.

a non-Newtonian (enthalpy) model – through the analysis of heat flow during rapid solidification of undercooled metal droplets. According to their models, the particle size r_0, the initial undercooling ΔT_n and the kinetic coefficient k_m have effects on interface profiles and velocities inside the droplets, of which the effect of the particle size is most notable for an alloy in an atomization process. Transition from convex to concave interface profile is produced by increasing the particle size r_0. If the interface profiles are regarded as isothermic inside the droplet at one moment, the isotherm influences the initial nuclei number and the nucleation sites because the nucleation takes place in the local position of lower temperature. For the particle of well-developed dendrite, in the study, the interface profiles are treated as in Fig. 7, where the interrupted line is expressed as isotherm. The droplets of interface convex toward liquid solidify from a single nucleation event, while the concave interface by multiple nucleation events, as shown in Figs 8 and 4.

4.3. Dendritic morphology versus the particle size

In the gas atomized powders, two β-dendrite – cellular dendrite and well-developed dendrites – are related to the undercooling, and the solidification undercooling depends strongly on the cooling rate and initial undercooling [1]. Because of the constitutional undulation among the droplets for the alloy with the high alloy content and/or more elements the nucleation temperature, which is related to the initial undercooling, is different for the droplets cooled with the cooling rate nearly equal.

In additions, the appearance of satellite sphere [12], i.e. some small particles attached to a big particle, can be found. The small particles (droplets) with faster cooling rate had solidified before attaching on the big one. As a nucleus, the small particles can raise the nucleation temperature of the big droplet. The cooling rate of the particles with same size does not keep constant, for the cooling environment such as gas velocities relative to droplets is not constant.

Therefore, in the big particles with small initial undercooling and low cooling rate, the latent heat released raises the temperature of liquid around the solid near solidus and restrains the growth of crystal. That limits the development of dendrite. Some secondary dendrite is broken into new nuclei by the undulation of constitutional and temperature during solidification. So those big particles solidify by multiple nucleation events and form a cellular-dendrite structure. The other particles with big initial undercooling or high cooling rate, for the undulation cannot breakdown secondary dendrite, either solidify by multiple nucleation events or from a single nucleation event, form well-developed dendrite structure.

5. Conclusion

For gas atomized Ti_3Al-based alloy Ti–25Al–10Nb–3V–1Mo powder with high pure argon, the solidification process and crystal morphologies vary mainly with the particle size. The results are as follows:

1. The cooling rate of $3 \times 10^3 \sim 4 \times 10^5$ K s^{-1} is obtained from the relationship of the cooling rate with secondary dendritic arm spacing, when the particle size is about 30 ~ 300 μm.
2. Two crystalline morphologies exist in big particles, cellular dendrite and well-developed dendrite, while the small particles are all of well-developed dendrite.
3. The big particles of cellular dendrite and well-developed dendrite solidify by multiple nucleation events, but the small particles of well-developed dendrite solidify from a single nucleation event.

4. The crystalline morphologies of gas-atomized Ti–35Al–10Nb–3V–1Mo powder are affected mainly by the particle size and the initial undercooling.
5. The microstructure of Ti–25Al–10Nb–3V–1Mo alloy is single β_0-phase prepared by gas atomization

References

1. T. Y. CHENG and S. H. ZHANG, "Rapid solidification technology and advanced materials" (Astronautic Press of China, Beijing, 1990) p. 85.
2. R. M. GERMAN, "Powder metallurgy science" (Metal Powder Industries Federation, Princeton, NJ, 1984) p. 32.
3. C. G. LEVI and R. MEHRABIAN. *Metall. Trans. B* **11B** (1980) 21.
4. *Idem*., *Metall. Trans. A* **13A** (1982) 221.
5. J. SHEN, *Doctoral dissertation*, Harbin Institute of Technology, Harbin, 1993 p. 45.
6. J. J. VALENCIA, C. McCULLOUGH, C. G. LEVI and R. MEHRABIAN, *Scripta Metall.* **21** (1987) 1341.
7. X. Z. CAI and D. EYLON, in Proceedings of the Eighth National Conference on Titanium and Its Alloy, China, 1993, (Institute of Steel and Iron Research, Shanghai, China, 1993) p. 355.
8. K. MURRALEEDHARAN, A. K. GOGIA, T. K. NANDY, D. BANERIEE and S. LELE, *Metall. Trans. A* **23A** (1992) 401.
9. R. STRYCHOR, J. C. WILLIAMS and W. A. SOFFA, *ibid.* **19A** (1988) 225.
10. M. J. AZIZ, *J. Appl. Phys.* **53** (1982) 1158.
11. J. W. CAHN, S. R. CORIELL and W. J. BOETTINGER, in "Laser and electron beam processing of materials", edited by C. W. White and P. S. Peercy (Academic Press, New York, 1980) p. 5.
12. Z. Q. HU and Y. H. ZHOU, "Essential of advanced materials for high technology " (Science nd Technology Press of China, Beijing, 1991) p. 210.

Received 18 October 1995
and accepted 20 January 1997